





Article

Investigation of NPB Analogs That Target Phosphorylation of BAD-Ser99 in Human Mammary Carcinoma Cells

Swamy Savvemala Girimanhanaika ^{1,†} , Dukanya Dukanya ^{1,†}, Ananda Swamynayaka ², Divya Maldepalli Govindachar ³, Mahendra Madegowda ², Ganga Periyasamy ³, Kanchugarakoppal Subbegowda Rangappa ⁶, Vijay Pandey ^{4,5}, Peter E. Lobie ^{4,5,7,*} and Basappa Basappa ^{1,*} 

- ¹ Laboratory Chemical Biology, Department of Studies in Organic Chemistry, University of Mysore, Manasagangotri, Mysore 570006, India; swamynayak010@gmail.com (S.S.G.); dukanya4@gmail.com (D.D.)
² Department of Studies in Physics, University of Mysore, Manasagangotri, Mysore 570006, India; anandas@physics.uni-mysore.ac.in (A.S.); mahen_xrdlab@yahoo.com (M.M.)
³ Department of Chemistry, Bangalore University, Bangalore 560056, India; divyamg03@gmail.com (D.M.G.); ganga.periyasamy@gmail.com (G.P.)
⁴ Tsinghua Berkeley Shenzhen Institute, Tsinghua Shenzhen International Graduate School, Tsinghua University, Shenzhen 518055, China; vijay.pandey@sz.tsinghua.edu.cn
⁵ Institute of Biopharmaceutical and Health Engineering, Tsinghua Shenzhen International Graduate School, Tsinghua University, Shenzhen 518055, China
⁶ Institution of Excellence, University of Mysore, Manasagangotri, Mysore 570006, India; rangappaks@gmail.com
⁷ Shenzhen Bay Laboratory, Shenzhen 518055, China
* Correspondence: pelobie@sz.tsinghua.edu.cn (P.E.L.); salundibasappa@gmail.com (B.B.)
† Equal contribution.



Citation: Girimanhanaika, S.S.; Dukanya, D.; Swamynayaka, A.; Govindachar, D.M.; Madegowda, M.; Periyasamy, G.; Rangappa, K.S.; Pandey, V.; Lobie, P.E.; Basappa, B. Investigation of NPB Analogs That Target Phosphorylation of BAD-Ser99 in Human Mammary Carcinoma Cells. *Int. J. Mol. Sci.* **2021**, *22*, 11002. <https://doi.org/10.3390/ijms222011002>

Academic Editors: Girolamo Ranieri and Clement G. Yedjou

Received: 11 July 2021

Accepted: 28 September 2021

Published: 12 October 2021

Publisher's Note: MDPI stays neutral with regard to jurisdictional claims in published maps and institutional affiliations.



Copyright: © 2021 by the authors. Licensee MDPI, Basel, Switzerland. This article is an open access article distributed under the terms and conditions of the Creative Commons Attribution (CC BY) license (<https://creativecommons.org/licenses/by/4.0/>).

Abstract: The design and development of a small molecule named NPB [3-((4(2,3-dichlorophenyl)piperazin-1-yl){2-hydroxyphenyl)methyl}-N-cyclopentylbenzamide], which specifically inhibited the phosphorylation of BAD at Ser99 in human carcinoma cells has been previously reported. Herein, the synthesis, characterization, and effect on cancer cell viability of NPB analogs, and the single-crystal X-ray crystallographic studies of an example compound (4r), which was grown via slow-solvent evaporation technique is reported. Screening for loss of viability in mammary carcinoma cells revealed that compounds such as 2[(4(2,3-dichlorophenyl)piperazin-1-yl)[naphthalen-1-yl]methyl]phenol (4e), 5[(4(2,3-dichlorophenyl)piperazin-1-yl)[2-hydroxyphenyl)methyl]uran-2-carbaldehyde (4f), 3[(2-hydroxyphenyl)[4(p-tolyl)piperazin-1-yl)methyl]benzaldehyde (4i), and NPB inhibited the viability of MCF-7 cells with IC₅₀ values of 5.90, 3.11, 7.68, and 6.5 μM, respectively. The loss of cell viability was enhanced by the NPB analogs synthesized by adding newer rings such as naphthalene and furan-2-carbaldehyde in place of N-cyclopentyl-benzamide of NPB. Furthermore, these compounds decreased Ser99 phosphorylation of hBAD. Additional in silico density functional theory calculations suggested possibilities for other analogs of NPB that may be more suitable for further development.

Keywords: BAD phosphorylation; Petasis reaction; lead optimization; drug design; human mammary carcinoma

1. Introduction

BCL-2-associated death promoter (BAD) is a modulator of apoptosis, which when unphosphorylated directly interacts with BCL-w, BCL-2, and BCL-xL, amongst other proteins [1]. Phosphorylation of BAD (pBAD) is required for its heterodimerization with 14-3-3 protein and promotion of cancer cell survival [2,3]. Specifically, the phosphorylation of human (h)BAD at Ser-75, Ser-99, and Ser-118 is required to promote cancer cell survival [4]. Human BAD is phosphorylated independently at Ser-75 and Ser-99 by RAS/RAF/MAPK and PI3K/AKT/mTOR pathways, respectively [5]. In addition, all three

PIM kinase family members may also phosphorylate hBAD on multiple sites but require prior phosphorylation of Ser-75 or Ser-99 and function as rescue kinases for BAD phosphorylation upon inhibition of RAS/RAF/MAPK and PI3/AKT/mTOR pathways [5–8]. Hence, as a common downstream cell survival mediator of both the RAS/RAF/MAPK and PI3K/AKT/mTOR pathways, phosphorylated BAD has been demonstrated to be critically involved in cancer development, progression, and therapeutic resistance. [5]. Therefore, pharmacological inhibition of BAD phosphorylation may be of utility to enhance therapeutic outcomes in oncology. Towards this goal, a novel bioactive small molecule called NPB [N-cyclopentyl-3-((4(2,3-dichlorophenyl)piperazin-1-yl){2-hydroxyphenyl} methyl) benzamide] was previously identified, which specifically inhibited the phosphorylation of hBAD on Ser-99 in various carcinoma cells independent of kinase activities [9,10]. Furthermore, NPB enhanced the efficacy of cisplatin in ovarian carcinoma and synergized with AZD5363, an AKT inhibitor in cisplatin resistant ovarian cancer [3]. Herein, the synthesis, characterization, and efficacy of newer NPB analogs with replacement of different substituents (R_1 , R_2 , and R_3) is reported (Figure 1) [11–16].

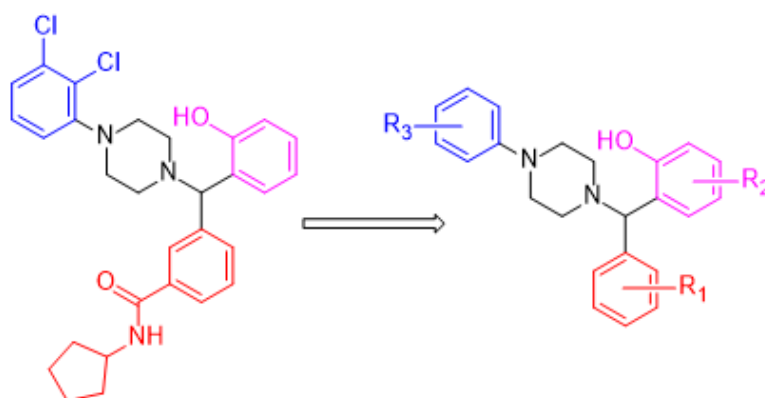
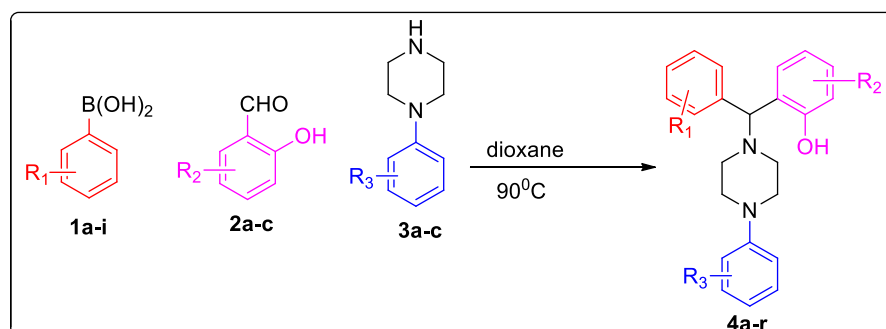


Figure 1. Changes in NPB structure after replacement with new R_1 , R_2 , and R_3 groups is shown.

2. Results and Discussion

The NPB analogs were synthesized based on the Petasis borono–Mannich reaction using N-substituted-piperazines, salicylaldehyde, and various boronic acids as the nucleophilic reagent [17–21]. In this multicomponent reaction, the iminium ion formation occurs initially, which reacts with boronic acid to form a tetracoordinate boronate in situ intermediate, and eventually the product formation occurs by intramolecular delivery of the organic group to iminium carbon (Scheme 1). The structures of all NPB analogs were characterized by LCMS, ^1H NMR, and ^{13}C NMR spectroscopic techniques (Table 1, refer supplementary spectra of all the compounds).



Scheme 1. Petasis reaction between substituted (R_3) phenyl piperazine, various (R_2) salicylaldehydes, and (R_1) different boronic acids to obtain NPB analogs ($4a-r$).

Table 1. Physical data and cell viability studies of NPB analogs in human mammary carcinoma (MCF-7 cells) cells.

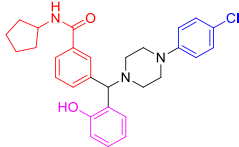
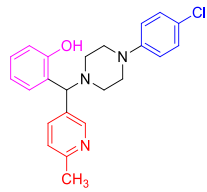
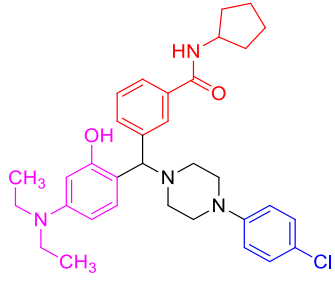
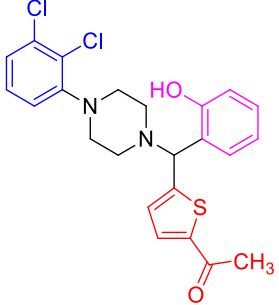
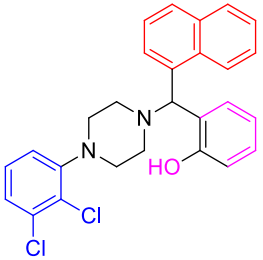
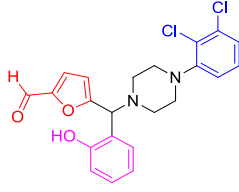
Entry	Structure	MCF-7 IC ₅₀ (μM)	Yield (%)	M.P (°C)
4a		605.6	91	128–130
4b		20.91	88	210–212
4c		23.83	81	178–180
4d		270.6	89	130–132
4e		5.90	78	78–80
4f		3.11	83	128–130

Table 1. Cont.

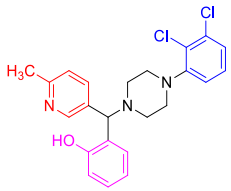
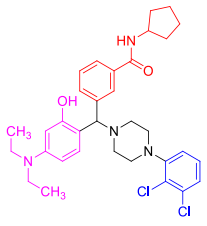
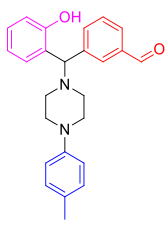
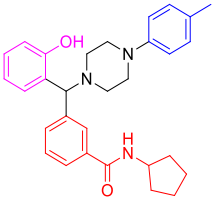
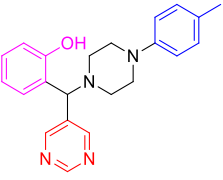
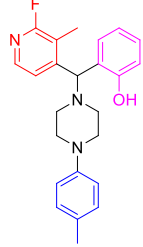
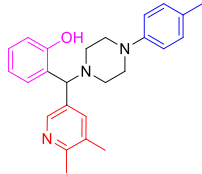
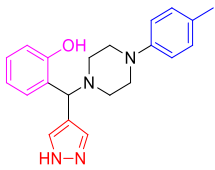
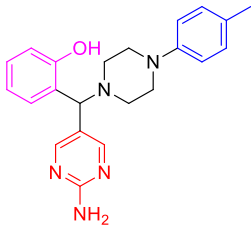
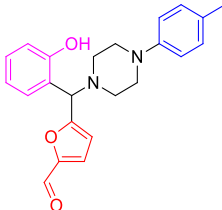
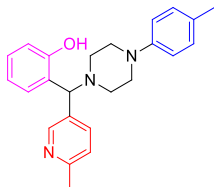
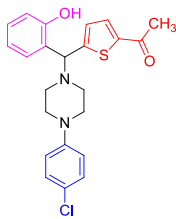
Entry	Structure	MCF-7 IC ₅₀ (μM)	Yield (%)	M.P (°C)
4g		-	83	208–210
4h		20.93	81	160–162
4i		7.68	88	120–123
4j		326.40	87	114–117
4k		221.50	84	157–161
4l		63.66	80	102–104

Table 1. Cont.

Entry	Structure	MCF-7 IC ₅₀ (μM)	Yield (%)	M.P (°C)
4m		45.73	86	147–159
4n		817.30	83	151–153
4o		1113.00	91	131–134
4p		156.00	87	94–97
4q		60.00	93	152–154
4r		-	89	140–142
	Doxorubicin	0.27		
	NPB	6.53		

Furthermore, the crystal structure of an example compound was determined using a slow evaporation technique [22]. Compound 4r emerged as a crystal and therefore its X-ray intensity data were recorded at a temperature of 293K on a Bruker AXS kappa Apex2 CCD Diffractometer, with a fine-focus sealed tube radiation source (MoK α) and

0.71073 Å wavelength. The procedure and reduction of the data set was accomplished using SAINT PLUS. SHELXS and SHELXL programs were adopted to solve and refine the structure, respectively [23,24]. The geometrical calculations, molecular figures, and crystal packing were generated and visualized by PLATON and MERCURY software, respectively (Table 2) [25]. CCDC number 2027110 contains full crystallographic data of **4r** and is available online at the Cambridge crystallographic data center. The ORTEP diagram was obtained for compound **4r** (Figure 2a). The crystal packing of the structure (Figure 2b) revealed the importance of the oxygen atom in the hydroxy group (i.e., present in all **4a-s**) and the chlorine atom in the para position of the phenyl ring (i.e., especially in the more potent compounds **4e** and **4f**), which confirms their participation in potential hydrogen bond formation via **O** and **Cl** atoms to form a three-dimensional supramolecular hydrogen-bonded network. This reflects the importance for compound stability and its role in interaction with other molecules. Such information is helpful in structure and activity relationships that provide a solid basis for structure-based optimization in the future design of further compounds. Structural analysis revealed that both phenyl and thiophene rings exhibited planar conformation, while the six-membered piperazine is in a chair conformation exhibiting puckering parameters: amplitude (Q) = 0.5535 Å, Θ = 4.61°, and Φ = 154.0425°. The planarity conformation of the phenyl and thiophene rings allows for the partial overlapping of aromatic rings, which play an important role in biological activity [26]. In addition, the hybridization of the C-C bond which is considered as one of the most important and common chemical elements, especially for organic connections, is usually formed by s and p orbitals of the second shell in carbon and lead to the formation of different bonds. Among several types of this hybridization, the **4r** molecule exhibited sp^2 hybridization that formed with two single bonds and one double bond between three atoms showing a 120° angle value between bonds. This type of hybridization was observed in phenyl and thiophene rings. On the other side, the piperazine ring exhibited sp^3 hybridization in which the carbon atom is bonded to four other atoms forming only a single bond. Here, 1s orbital and 3p orbitals in the same shell of an atom combine to form four new equivalent orbitals. The presence of different types of hybridization enhances the bond strength, stability, and reactivity of the molecule.

Table 2. Crystal data and structure refinement details of **4r** molecule.

CCDC No	2027110
Empirical formula	C ²³ H ²³ Cl N ² O ² S
Formula weight	426.94
Temperature	293 K
Wavelength	0.71073 Å
Reflns. for cell determination	1802
θ range for above	3.643° to 58.989°
Crystal system	<i>P</i> -1
Space group	Triclinic
Cell dimensions	a = 11.4518(8) Å, b = 13.5450(10) Å, c = 14.7351(7) Å α = 101.790(4)°, β = 102.701(4)°, γ = 96.286(4)°
Volume	2153.8(2) Å ³
Z	4
F ₀₀₀	896
θ range for data collection	2.215° to 25.827°
Index ranges	-14 < h < 14; -16 < k < 16; -18 < l < 18
Reflections collected	43,360
Independent reflections	8277
Refinement method	Full-matrix least-squares on F ²
Data/restraints/parameters	8277/36/538
Goodness-of-fit on F ²	1.015
Final [I > 2 σ (I)]	R1 = 0.0545, wR2 = 0.1249
R indices (all data)	R1 = 0.1243, wR2 = 0.1639
Largest diff. peak and hole	0.333 and -0.536 e Å ⁻³

** Carbonyl group of one molecule with disorder sites of occupancy ratio of 0.23 and 0.77 were refined with SADI/SAME/SIMU SHELXL instructions.

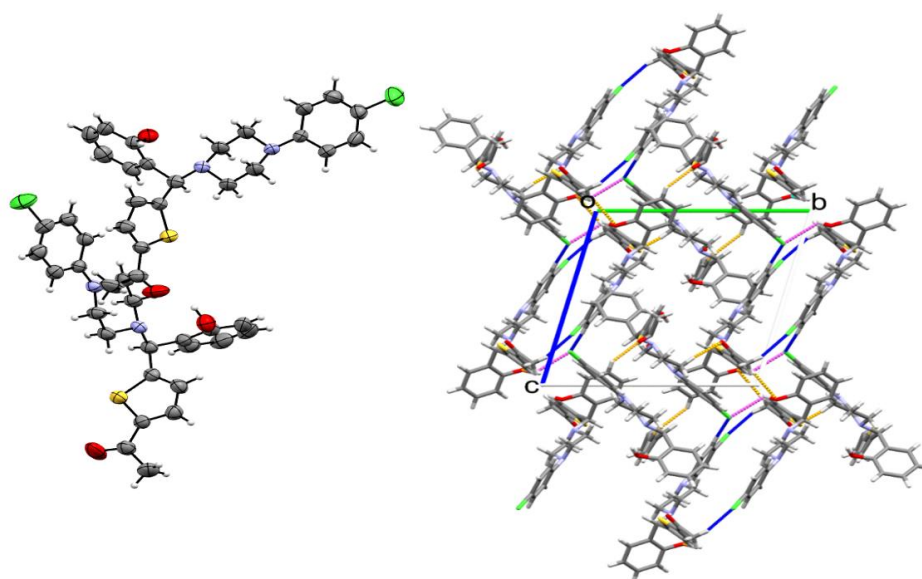


Figure 2. (a) ORTEP structure of compound **4r**. (b) structure of crystal packing viewed down *a* axis, showing hydrogen bonds colorized as (i) C-H... Cl (blue), (ii) O-H... Cl (pink) and (iii) C-H... O (orange).

Since NPB was previously reported to inhibit the viability of various carcinoma cells, its analogs were tested for their ability to inhibit mammary carcinoma cell viability using the reported protocol [27,28]. The results of the study revealed that the compounds such as 2[(4(2,3-dichlorophenyl)piperazin-1-yl)[naphthalen-1-yl]methylphenol (**4e**), 5[(4(2,3-dichlorophenyl)piperazin-1-yl)[2-hydroxyphenyl]methylfuran-2-carbaldehyde (**4f**), 3[(2-hydroxyphenyl)4(p-tolyl)piperazin-1-yl]methylbenzaldehyde (**4i**) as well as NPB inhibited the viability of MCF-7 cells with an IC_{50} values of 5.9, 3.11, 7.68, and 6.53 μM , respectively (Table 1). Interestingly, the compounds **4e**, **4f**, **4i**, and NPB inhibited the viability of normal breast cell MCF10A, with higher IC_{50} values of 33.8, 61.4, 28.5, and 110.6 μM , respectively. The NPB analogs synthesized by adding newer substituents such as naphthalene and furan-2-carbaldehyde in place of N-cyclopentylbenzamide of NPB slightly enhanced the loss of cell viability in MCF-7 cells. It was important to note that the dichlorophenyl group in NPB and its analogs seems quite important; however, some of the tested NPB analogs, which were synthesized by replacing the dichlorophenyl, and N-cyclopentylbenzamide group of NPB with 4-p-tolyl-group and benzaldehyde substitution, also exhibited enhanced loss of cell viability. Among 4-chloro-phenyl group containing piperazine compounds, **4b** and **4c** showed better inhibitory effects on viability of MCF-7 cells with IC_{50} values of 20.91 and 23.83 μM , whereas for the tolyl group added piperazine compounds such as **4l** and **4m**, IC_{50} values were observed to be 63.66, and 45.73 μM , respectively.

As the tested NPB analogs produced loss of cell viability to variable extents in mammary carcinoma cells, *in silico* density functional theory calculations were performed in order to understand the structure activity relationship of NPB analogs against the loss of cell viability (Supplementary Figure S1). The highest occupied molecular orbital (HOMO) and lowest unoccupied molecular orbital (LUMO) energy values showed the electron donating and accepting ability of NPB analogs, respectively. Computed HOMO and LUMO eigen functions indicated that the donor–acceptor nature of NPB analogs localized with MOs at different regions (Figures 3 and 4). Therefore, the substitutions at both ends were observed to significantly alter the electronic density levels. The computed data indicated that IC_{50} decreases with decreasing E_{HOMO} for NPB analogs, which bear electronically similar functional groups. Calculated HOMO and LUMO values are in the range of -5 to -6.5 eV and -1.5 to 2.5 eV (Table 3). Molecular electrostatic potential shows the charge separation between the two ends within the molecule. Improved loss of cell viability is observed with NPB analogs which possess similar functional groups. Hence, the NPB

analogues, which possess electron donor function as three separate classes, were analyzed. In the first set, amongst the tested compounds, i.e., **4a**, **4b**, **4c** and **4r**, the compound **4b** has comparatively lower E_{HOMO} of -6.16 eV and E_{LUMO} of -2.70 eV values. Due to the relatively smaller HOMO-LUMO gaps, electronegativity and electrophilicity values, and chemical hardness of **4b**, the lower the observed IC_{50} in mammary carcinoma cells. In the second class of NPB analogues, namely **4d**, **4e**, **4f**, **4g**, and **4h**, the activities are arranged in ascending order of E_{HOMO} and E_{LUMO} values, i.e., $4g < 4d < 4h < 4e < 4f$, which is in accordance with their respective IC_{50} values (Figure 5). In the last class of tolyl group containing molecules such as **4i**, **4j**, **4k**, **4l**, **4m**, **4n**, **4o**, **4p**, and **4q**, the molecule **4i** found to be highly effective against MCF-7 cells, which possess lower electronic factors compared to the other similar functional group tagged molecules. DFT studies predicted the activity of the molecule in line with experimental predictions. Among the molecules studied here, **4f** exhibits higher activity than other molecules.

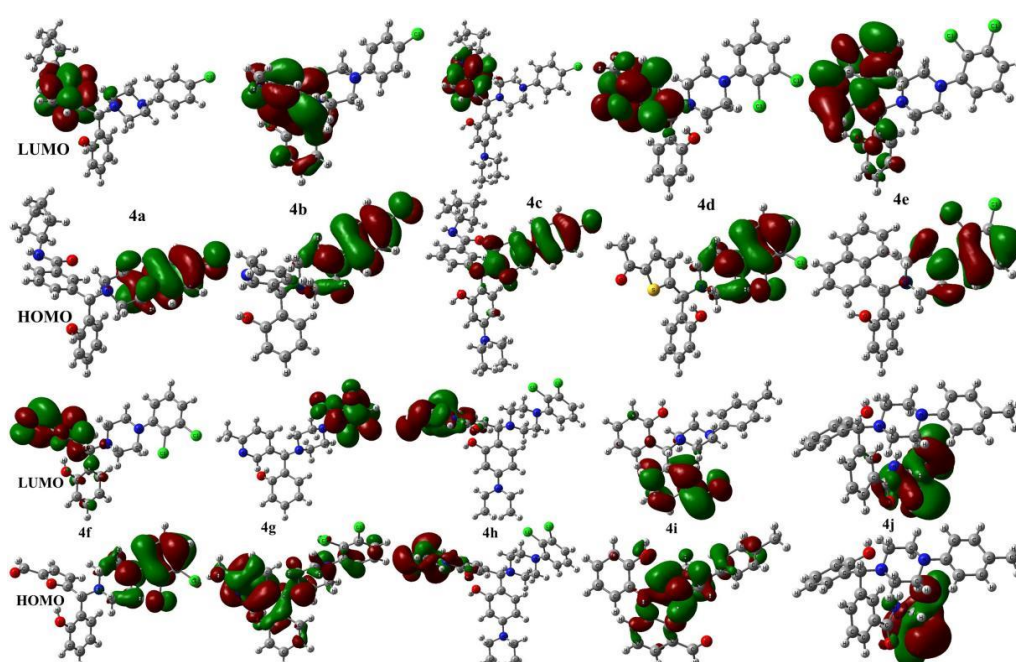


Figure 3. Computed molecular orbital plots for synthesized molecules **4a-4j** with the counter value of 0.02 \AA^{-3} .

Table 3. Computed E_{HOMO} , E_{LUMO} , HOMO-LUMO gap (Δ), chemical hardness (η), electronegativity (χ), and electrophilicity index (ω) in eV for all the synthesized molecules.

Entry	E_{HOMO}	E_{LUMO}	Δ	η	χ	ω
4a	-5.87	-1.55	4.32	2.16	3.71	3.19
4b	-6.16	-2.68	3.48	1.74	4.42	5.60
4c	-5.71	-1.52	4.19	2.10	3.61	3.11
4r	-5.91	-2.25	3.66	1.83	4.08	4.55
4d	-5.36	-1.96	3.40	1.70	3.66	3.93
4e	-6.48	-4.49	1.98	0.99	5.48	15.16
4f	-6.50	-4.89	1.61	0.80	5.69	20.14
4g	-5.24	-1.18	4.05	2.03	3.21	2.54
4h	-5.75	-2.90	2.85	1.43	4.32	6.55
4i	-5.92	-2.65	3.27	1.64	4.28	5.61
4j	-4.97	-1.64	3.33	1.66	3.31	3.29
4k	-5.26	-1.65	3.60	1.80	3.46	3.31
4l	-5.64	-2.06	3.58	1.79	3.85	4.14
4m	-5.67	-2.10	3.56	1.78	3.88	4.23
4n	-4.68	-1.58	3.10	1.55	3.13	3.16
4o	-3.97	-1.42	2.55	1.27	2.69	2.84
4p	-5.51	-2.02	3.49	1.74	3.77	4.07
4q	-5.69	-2.11	3.57	1.79	3.90	4.26

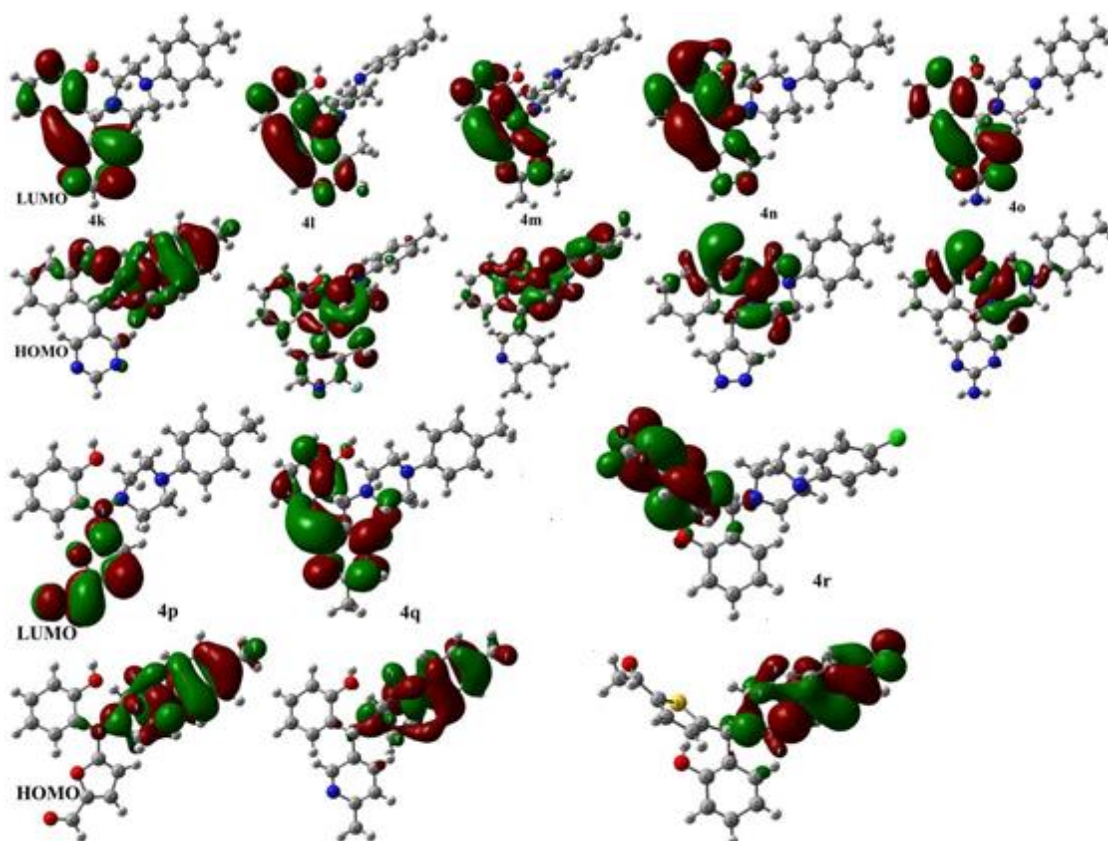


Figure 4. Computed molecular orbital plots for synthesized molecules 4k-4r with the counter value of 0.02 \AA^{-3} .

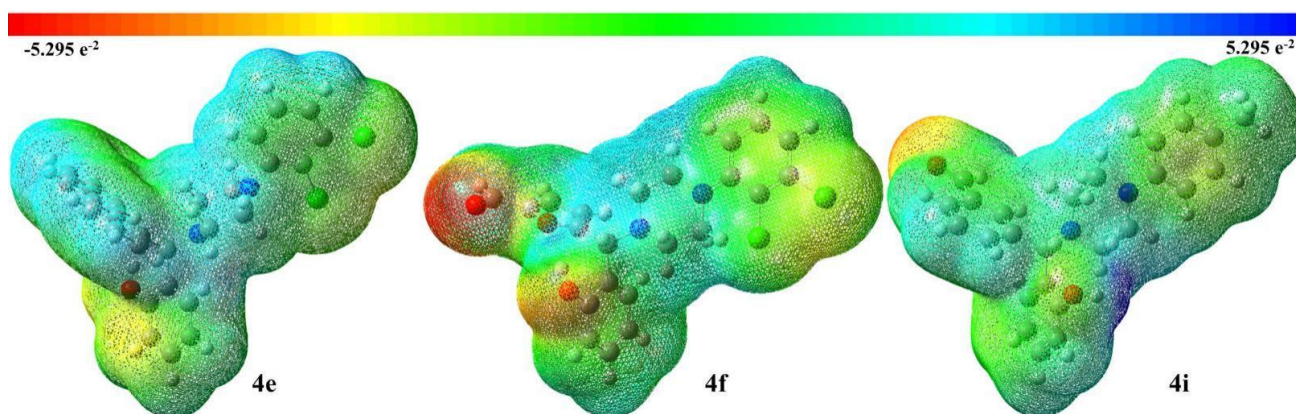


Figure 5. Molecular electrostatic charge distribution plots for 4e, 4f and 4i (highly active molecules) with an isovalue of 0.004 \AA^{-3} .

As phosphorylation of hBAD at Ser-99 promotes cancer cell survival and NPB was reported to specifically inhibit BAD-Ser99 phosphorylation, western blot analysis was performed to evaluate the efficacy of the most active NPB analogs (4f, 4e, and 4i) on BAD-Ser99 phosphorylation in MCF-7 cells. All the tested compounds decreased the pBAD at Ser-99 without change in total BAD expression (Figure 6).

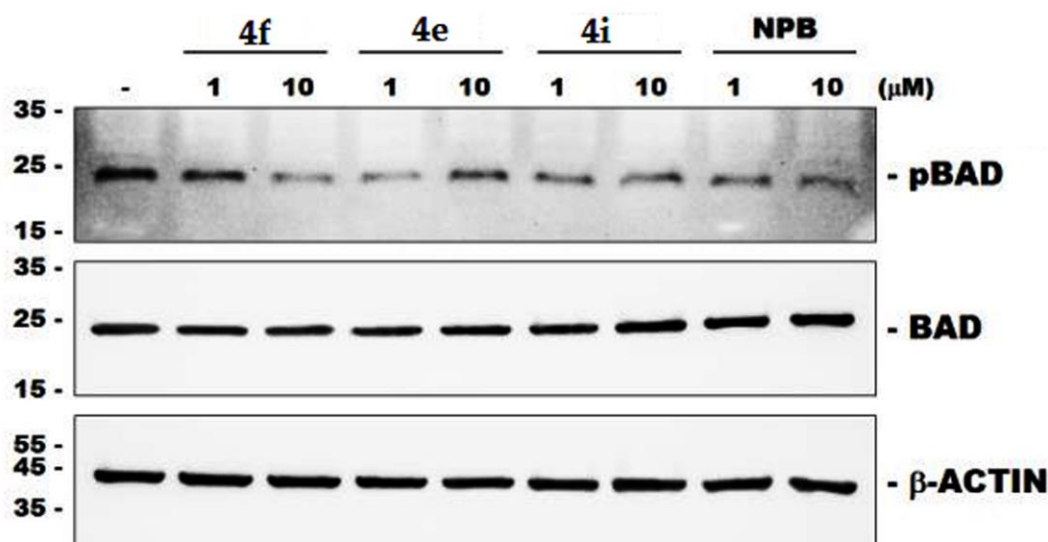


Figure 6. Western blot analysis of expression of hBAD (BAD) and Ser-99 phosphorylation (pBAD) of hBAD after treatment of MCF-7 cells with NPB analogs (**4f**, **4e**, and **4i**). β -ACTIN was used as input control.

Since the active compounds (**4e**, **4f**, **4i**, and **NPB** as a comparison) displayed efficacy against MCF-7 cells, the in silico ADMET properties (8 parameters) of these compounds were determined by using vNN-ADMET online platform [29]. The results are tabulated in Table 4. The in silico analyses of active compounds predicted that the compounds (**4e**, **4f**, **4i**) would not exhibit hepatotoxicity.

Table 4. The vNN-ADMET predictions for active compounds **4e**, **4f** and **4i**.

Query	Liver Toxicity		Metabolism					
	DILI	CT	CYP Inhibitors for					
			HLM	1A2	3A4	2D6	2C9	2C19
4e	N ^a	Y ^b	N	N	N	N	N	N
4f	N	Y	Y	N	N	N	N	N
4i	N	N	Y	N	N	N	N	N
NPB	Y	N	Y	N	N	N	N	N

Note: Y^b, Yes; N^a, No; DILI, drug-induced liver injury; CT, cytotoxicity; CYP, cytochrome P450; HLM, human liver microsomes. Predictions and interpretations using online server and a restricted/unrestricted applicability domain are represented.

3. Materials and Methods

Materials and reagents were purchased from commercial suppliers and used as instructed. Melting points were determined through an open capillary method using Sigma melting point apparatus (Sigma, Bangalore, India) and are uncorrected. IR spectra were recorded on Shimadzu IR spectrophotometer (Shimadzu USA manufacturing Inc., Canby, OR, USA). ¹H NMR and ¹³C NMR spectra were recorded on Bruker/Agilent NMR spectrometer operating at 400 and 100 MHz, respectively, using TMS as internal standard; chemical shifts are in *d*. Mass spectroscopic analysis was performed on Shimadzu LC-MS. Analytical TLCs were implemented on pre-coated Merck 0.25 mm silica gel 60F254 plates using 40% ethylacetate in *n*-hexane as eluent and the spots were detected under UV light. All other chemicals were of analytical grade and were purchased from Sisco Research Laboratories (SRL, Mumbai, India).

General procedure for synthesis of NPB analogs. The piperazines (**1eq**) and salicylaldehydes (**1eq**) were taken in a round bottom flask and stirred with dioxane as a solvent for 10 min. After 10 min the aryl boronic acid (**1eq**) was added to the mixture and refluxed

for 8 h on a hot plate at 90 °C with continuous stirring. After 8 h, ethyl acetate and water were added to the reaction mixture, separating the ethyl acetate layer using a separate funnel, and drying over anhydrous sodium sulphate. Ethyl acetate was evaporated to produce the product. The desired phenolic compound product was obtained by column chromatography [10].

Characterization of 3(4(4-chlorophenyl)piperazin-1-yl) (2-hydroxyphenyl)methyl)-N-cyclopentylbenzamide (4a) Off-white solid; mp 128–130 °C; 91% yield; ¹H NMR (CDCl₃, 400 MHz) δ: 11.49 (s, 1H), 7.84 (s, 1H), 7.64–7.59 (m, 2H), 7.36 (t, *J* = 8 Hz, 1H), 7.19 (d, *J* = 4 Hz, 2H), 7.14 (t, *J* = 8 Hz, 2H), 6.96 (d, *J* = 4 Hz, 1H), 6.87 (d, *J* = 8 Hz, 1H), 6.79 (d, *J* = 8 Hz, 1H), 6.75–6.72 (m, 1H), 6.10 (s, 1H), 4.53 (s, 1H), 4.41–4.36 (m, 1H), 3.20 (s, 4H), 2.83–2.59 (m, 4H), 2.08 (s, 2H), 1.73–1.65 (m, 2H), 1.52–1.42 (m, 2H), 1.34–1.26 (m, 2H); ¹³C NMR (CDCl₃, 100 MHz) δ: 166.8, 156.2, 149.4, 140.3, 135.6, 131.1, 129.3, 129.1, 128.9, 127.6, 126.3, 125.2, 124.6, 119.8, 117.8, 117.2, 114.5, 76.1, 51.9, 51.6, 49.3, 33.2. 23.8; HRMS (ESI-TOF) *m/z*: [M+H]⁺ calcd for C₂₉H₃₂ClN₃O₂, 490.2261; found, 490.2259.

Characterization of 2(4(4-chlorophenyl)piperazin-1-yl) (6-methylpyridin-3-yl)methylphenol (4b) Off-white solid; mp 210–212 °C; 88% yield; ¹H NMR (CDCl₃, 400 MHz) δ: 11.50 (br-s, 1H) 8.55 (s, 1H) 7.80–7.78 (m, 1H) 7.26–7.15 (m, 4H) 6.99 (d, *J* = 8 Hz, 1H) 6.93 (d, *J* = 8 Hz, 1H) 6.86–6.79 (m, 3H) 4.55 (s, 1H) 3.33–3.22 (m, 4H) 2.82–2.66 (m, 4H) 2.56 (s, 3H); ¹³C NMR (CDCl₃, 100 MHz) δ: 158.7, 156.2, 149.4, 149.2, 136.2, 132.0, 129.2, 129.1, 125.3, 124.3, 123.8, 119.8, 117.7, 117.7, 117.3, 73.2, 51.5, 49.3, 24.1; HRMS (ESI-TOF) *m/z*: [M+H]⁺ calcd for C₂₃H₂₄ClN₃O, 394.1686; found, 394.1682.

Characterization of 3(4(4-chlorophenyl)piperazin-1-yl) (4(diethylamino)-2-hydroxyphenyl)methyl)-N-cyclopentylbenzamide (4c) Brown solid; mp 178–180 °C; 81% yield; ¹H NMR (CDCl₃, 400 MHz) δ: 11.23 (br-s, 1H), 7.78 (s, 1H), 7.97 (d, *J* = 8 Hz, 2H), 7.38–7.34 (m, 1H), 7.18 (d, *J* = 8 Hz, 2H), 6.80–6.73 (m, 2H), 6.18 (s, 1H), 6.08–6.01 (m, 2H), 4.44 (s, 1H), 4.39 (s, 1H), 3.30–3.27 (m, 4H), 3.25–3.19 (m, 4H), 2.62–2.52 (m, 2H), 2.06–2.10 (m, 3H), 1.71–1.48 (m, 8H), 1.12 (t, *J* = 8 Hz, 6H); ¹³C NMR (CDCl₃, 100 MHz) δ: 166.9, 157.1, 149.5, 148.9, 141.0, 135.4, 131.2, 129.9, 129.7, 129.1, 127.3, 125.9, 124.9, 117.3, 111.6, 103.5, 99.7, 75.4, 51.8, 51.4, 49.3, 44.2, 33.2, 23.8, 12.7; HRMS (ESI-TOF) *m/z*: [M+H]⁺ calcd for C₃₃H₄₁ClN₄O₂, 561.2996; found, 561.2998.

Characterization of 1(5((4(2,3-dichlorophenyl)piperazin-1-yl) (2-hydroxyphenyl)methyl)thiophen-2-yl)ethanone (4d) White solid; mp 130–132 °C; 89% yield; ¹H NMR (CDCl₃, 400 MHz) δ: 11.14 (br-s, 1H) 7.60 (d, *J* = 4 Hz, 1H) 7.25–7.17 (m, 4H) 7.06–6.93 (m, 3H) 6.84–6.80 (m, 1H) 4.87 (s, 1H) 3.19–3.16 (m, 4H) 2.89–2.79 (m, 4H) 2.55 (s, 3H); ¹³C NMR (CDCl₃, 400 MHz) δ: 190.5, 155.9, 150.6, 150.5, 144.4, 134.2, 132.4, 129.5, 128.9, 127.7, 127.6 (2C), 125.1, 124.0, 119.8, 118.7, 117.4, 70.6, 51.5, 51.2, 26.7; LCMS *m/z*: [M+H]⁺ calcd for C₂₃H₂₂Cl₂N₂O₂S, 461.0857; found, 460.9520.

Characterization of 2-((4(2,3-dichlorophenyl)piperazin-1-yl)(naphthalen-1-yl)methyl)phenol (4e). Brown solid; mp 78–80 °C; 78% yield; ¹H NMR (CDCl₃, 400 MHz) δ: 8.08 (d, *J* = 8 Hz, 1H) 7.91–7.74 (m, 3H) 7.93–7.33 (m, 2H) 7.22–7.14 (m, 2H) 6.98 (d, *J* = 8 Hz, 1H) 6.90–6.83 (m, 1H) 6.78–6.55 (m, 3H) 6.60–6.59 (m, 1H) 5.37 (s, 1H) 4.23 (s, 1H) 3.37–3.28 (m, 4H) 3.04–2.33 (m, 4H); ¹³C NMR (CDCl₃, 100 MHz) δ: 155.8, 154.8, 136.7, 135.1, 134.1, 131.1, 130.9, 129.3, 129.2, 128.9, 128.6, 128.4, 126.1, 125.8, 125.4, 124.1, 123.7, 120.6, 119.9, 117.0, 116.9, 74.0, 52.7, 52.5; HRMS (ESI-TOF) *m/z*: [M+H]⁺ calcd for C₂₇H₂₄Cl₂N₂O, 463.1343; found, 463.1340.

Characterization of 5(4(2,3-dichlorophenyl)piperazin-1-yl) (2-hydroxyphenyl)methylfuran-2-carbaldehyde (4f) Brown solid; mp 128–130 °C; 83% yield; ¹H NMR (CDCl₃, 400 MHz) δ: 10.06 (s, 1H) 8.20 (s, 1H) 8.07–7.90 (m, 1H) 7.74–7.44 (m, 2H) 7.20–7.12 (m, 1H) 6.96–6.87 (m, 1H) 6.35–6.33 (m, 1H) 6.21–6.12 (m, 1H) 5.29 (s, 1H) 4.41 (s, 1H), 3.41–3.04 (m, 4H) 2.34–2.10 (m, 4H); ¹³C NMR (CDCl₃, 100 MHz) δ: 177.6, 158.4, 156.7, 152.4, 150.4, 134.1, 129.8, 128.9, 127.6, 127.5, 125.1, 121.9, 121.3, 119.8, 111.6, 117.2, 112.0, 67.7, 51.2, 50.6; HRMS (ESI-TOF) *m/z*: [M+H]⁺ calcd for C₂₂H₂₀Cl₂N₂O₃, 431.0929; found, 431.0924

Characterization of 2(4(2,3-dichlorophenyl)piperazin-1-yl) (6-methylpyridin-3-yl)methyl)phenol, 4g Yellow solid; mp 208–210 °C; 83% yield; ¹H NMR (CDCl₃, 400 MHz) δ: 11.50 (br-s, 1H), 8.55 (s, 1H), 7.80–7.77 (m, 1H), 7.25–7.16 (m, 4H), 7.00–6.78 (m, 4H), 4.55 (s, 1H), 3.26 (s, 4H), 2.81–2.66 (m, 4H), 2.58 (s, 3H); ¹³C NMR (CDCl₃, 100 MHz) δ: 158.7, 156.2, 149.4, 149.2, 136.1, 132.0, 129.5, 129.1, 129.0, 125.2, 124.3, 124.1, 124.0, 123.8, 119.8, 117.5, 117.3, 73.2, 51.5, 49.3, 24.1; HRMS (ESI-TOF) m/z: [M+H]⁺ calcd for C₂₃H₂₃Cl₂N₃O, 428.3542; found, 428.0576.

Characterization of N-cyclopentyl-3(4(2,3-dichlorophenyl)piperazin-1-yl) (4(diethylamino)-2-hydroxyphenyl)methyl)benzamide, 4h White solid; mp 160–162 °C; 81% yield; ¹H NMR (CDCl₃, 400 MHz) δ: 7.78 (s, 1H), 7.58–7.56 (m, 1H), 7.38–7.34 (m, 1H), 7.18 (d, J = 8 Hz, 2H), 6.80–6.73 (m, 2H), 6.18 (s, 1H), 6.09–6.00 (m, 2H), 4.44 (s, 1H), 4.41–4.34 (m, 1H), 3.40–3.19 (m, 6H), 3.19–3.10 (m, 2H); ¹³C NMR (CDCl₃, 100 MHz) δ: 168.4, 154.6, 149.4, 137.5, 133.8, 132.5, 128.9, 128.4, 128.2, 127.4, 127.0, 126.6, 125.8, 125.6, 119.2, 118.5, 110.2, 103.4, 101.2, 68.2, 51.5, 48.8, 44.8, 33.2, 29.6, 24.3, 13.1; HRMS (ESI-TOF) m/z: [M+H]⁺ calcd for C₃₃H₄₀Cl₂N₄O₂, 595.2606; found, 595.2601.

Characterization of 3(2-hydroxyphenyl) (4(p-tolyl)piperazin-1-yl)methyl)benzaldehyde, 4i Brown; mp 120–123 °C; 88% yield; ¹H NMR (CDCl₃, 400 MHz) δ: 11.66 (s, 1H), 10.03 (s, 1H), 7.97 (s, 1H), 7.83 (d, J = 8 Hz, 2H), 7.55–7.52 (m, 1H), 7.20–7.17 (m, 1H), 7.10 (d, J = 8 Hz, 2H), 7.00 (d, J = 8 Hz, 1H), 6.92 (d, J = 8 Hz, 1H), 6.86 (d, J = 8 Hz, 2H), 6.80–6.77 (m, 1H), 4.62 (s, 1H), 3.25 (s, 4H), 2.66 (s, 4H), 2.29 (s, 3H); ¹³C NMR (CDCl₃, 100 MHz) δ: 192.3, 156.4, 148.8, 141.2, 137.2, 134.6, 130.1, 130.0, 129.9, 129.5, 129.3, 124.7, 120.0, 117.6, 116.8, 76.2, 52.0, 50.0, 50.1, 20.7; LCMS m/z: [M+H]⁺ calcd for C₂₅H₂₆N₂O₂, 386.1994; found, 387.2418.

Characterization of N-cyclopentyl-3(2-hydroxyphenyl) (4(p-tolyl)piperazin-1-yl)methyl)benzamide (4j); Brown; mp: 114–117 °C; 87% yield; ¹H NMR (CDCl₃, 400 MHz) δ: 11.72 (s, 1H), 7.87 (s, 1H), 7.64 (d, 2H, J = 8 Hz), 7.39 (t, 1H, J = 6 Hz), 7.16 (t, 1H, J = 6 Hz), 7.10 (d, 2H, J = 8 Hz), 6.86 (m, 5H), 6.16 (s, 1H), 4.57 (s, 1H), 4.41 (m, 1H), 3.23 (s, 4H), 2.63 (s, 4H), 2.30 (s, 3H), 2.12 (s, 2H), 1.72 (m, 4H), 1.53 (m, 2H); ¹³C NMR (CDCl₃, 100 MHz) δ: 166.8, 156.2, 148.6, 140.4, 135.5, 131.1, 129.8, 129.7, 129.3, 128.8, 127.9, 126.3, 124.7 (2C), 119.7, 117.2, 116.6, 76.1, 51.8, 49.8, 33.2, 29.7, 29.4, 23.8, 20.5; HRMS (ESI-TOF); m/z: [M+H]⁺ calcd for C₃₀H₃₅N₃O₂, 469.2729; found, 469.2726.

2(pyrimidin-5-yl) (4(p-tolyl)piperazin-1-yl)methyl)phenol (4k); Off-white solid; mp: 157–161 °C; 84% yield; ¹H NMR (CDCl₃, 400 MHz) δ: 9.16 (s, 1H), 8.84 (s, 2H), 7.19 (t, 1H, J = 4 Hz), 7.07 (d, 2H, J = 4 Hz), 6.92 (m, 2H), 6.81 (m, 3H), 4.50 (s, 1H), 3.89 (s, 1H), 3.20 (m, 4H), 2.74 (m, 4H), 2.27 (s, 3H); ¹³C NMR (CDCl₃, 100 MHz) δ: 158.7, 157.1, 156.2, 148.5, 130.6, 130.3, 129.9, 129.9, 129.8, 128.9, 127.7, 123.2, 120.3, 117.8, 117.2, 116.8, 71.8, 51.9, 49.9, 29.8, 20.6, 14.2; HRMS (ESI-TOF) m/z: [M+H]⁺ calcd for C₂₂H₂₄N₄O; 360.1950 found, 360.1953.

Characterization of 2(2-fluoro-3-methylpyridin-4-yl) (4(p-tolyl)piperazin-1-yl)methyl)phenol (4l); Yellow solid; mp: 102–104 °C; 80% yield; ¹H NMR (CDCl₃, 400 MHz) δ: 8.00 (d, 1H, J = 4 Hz), 7.54 (d, 1H, J = 4 Hz), 7.19 (t, 1H, J = 4 Hz), 7.10 (d, 2H, J = 8 Hz), 6.96 (d, 1H, J = 8 Hz), 6.92 (d, 1H, J = 8 Hz), 6.84 (d, 2H, J = 4 Hz), 6.78 (t, 1H, J = 4 Hz), 4.94 (s, 1H), 3.23 (s, 6H), 2.47 (s, 4H), 2.29 (s, 4H); ¹³C NMR (CDCl₃, 100 MHz) δ: 163.4, 161.5, 156.1, 148.4, 145.0, 144.9, 129.7, 129.3, 128.6, 123.4, 120.1, 119.8, 117.5, 116.6, 68.9, 49.8, 49.6, 20.3, 11.35; HRMS (ESI-TOF) m/z: [M+H]⁺ calcd for C₂₄H₂₆FN₃O, 391.2060; found, 391.2057.

Characterization of 2(5,6-dimethylpyridin-3-yl) (4(p-tolyl)piperazin-1-yl)methyl)phenol (4m); Off-white solid; mp: 147–159 °C; 86% yield; ¹H NMR (CDCl₃, 400 MHz) δ: 11.66 (s, 1H), 8.34 (s, 1H), 7.56 (s, 1H), 7.15 (t, 1H, J = 4 Hz), 7.07 (d, 2H, J = 8 Hz), 6.94 (d, 1H, J = 4 Hz), 6.89 (d, 1H, J = 8 Hz), 6.81 (d, 2H, J = 4 Hz), 6.75 (t, 1H, J = 4 Hz), 4.48 (s, 1H), 3.21 (s, 4H), 2.62 (s, 3H), 2.26 (d, 6H, J = 8 Hz); ¹³C NMR (CDCl₃, 100 MHz) δ: 157.4, 156.2, 148.6, 146.4, 132.6, 129.7, 129.1, 128.8, 124.4, 119.6, 117.2, 116.6, 73.2, 49.8, 29.6, 22.2, 20.4, 19.3; HRMS (ESI-TOF) m/z: [M+H]⁺ calcd for C₂₅H₂₉N₃O, 387.2311; found, 387.2316.

Characterization of 2(1H-pyrazol-4-yl) (4(p-tolyl)piperazin-1-yl)methyl)phenol (4n); Off-white solid; mp: 151–153 °C; 83% yield; ¹H NMR (CDCl₃, 400 MHz) δ: 7.59 (s, 2H), 7.15 (t, 1H, J = 8 Hz), 7.05 (d, 2H, J = 8 Hz), 6.94 (d, 1H, J = 8 Hz), 6.87 (d, 1H, J = 8 Hz), 6.80 (d, 2H,

$J = 8\text{Hz}$), 6.74 (t, 1H, $J = 4\text{Hz}$), 4.63 (s, 1H), 3.14 (d, 4H, $J = 8\text{Hz}$), 2.67 (s, 4H), 2.25 (s, 3H); ^{13}C NMR (CDCl_3 , 100MHz) δ : 156.5, 148.6, 133.7, 129.8, 129.6, 128.8, 128.6, 125.4, 119.3, 118.0, 116.8, 116.6, 65.6, 50.7, 49.8, 29.6, 20.4; HRMS (ESI-TOF) m/z : $[\text{M}+\text{H}]^+$ calcd for $\text{C}_{21}\text{H}_{24}\text{N}_4$, 332.2001; found, 332.2005.

Characterization of 2(2-aminopyrimidin-5-yl) (4(p-tolyl)piperazin-1-yl)methyl phenol (4o); Yellow solid; mp: 131–134 °C; 91% yield; ^1H NMR (CDCl_3 , 400MHz) δ : 8.32 (s, 2H), 7.16 (t, 1H, $J = 6\text{Hz}$), 7.05 (d, 2H, $J = 8\text{Hz}$), 6.88 (t, 2H, $J = 6\text{Hz}$), 6.77 (m, 3H), 5.44 (s, 2H), 4.36 (s, 1H), 3.19 (s, 4H), 2.65 (s, 4H), 2.25 (s, 3H); ^{13}C NMR (CDCl_3 , 100MHz) δ : 162.8, 158.6, 156.3, 148.4, 129.9, 129.7, 129.0, 128.7, 123.8, 122.2, 119.7, 117.3, 116.6, 51.3, 49.8, 20.4; HRMS (ESI-TOF) m/z : $[\text{M}+\text{H}]^+$ calcd for $\text{C}_{22}\text{H}_{25}\text{N}_5\text{O}$, 375.2059; found, 375.2056.

Characterization of 5(2-hydroxyphenyl) (4(p-tolyl)piperazin-1-yl)methylfuran-2-carbaldehyde (4p); Off-white solid; mp 94–97 °C; 87% yield; ^1H NMR (CDCl_3 , 400MHz) δ : 10.9 (s, 1H), 9.62 (s, 1H), 7.22 (t, 1H, $J = 4\text{Hz}$), 7.07 (d, 2H, $J = 4\text{Hz}$), 6.95 (d, 1H, $J = 8\text{Hz}$), 6.91 (d, 1H, $J = 8\text{Hz}$), 6.81 (t, 1H, $J = 4\text{Hz}$), 6.62 (s, 1H), 4.82 (s, 1H), 3.20 (s, 4H), 2.75 (s, 4H), 2.27 (s, 3H); ^{13}C NMR (CDCl_3 , 100MHz) δ : 177.9, 158.8, 157.1, 152.7, 148.8, 130.5, 130.1, 130.1, 129.2, 121.7, 120.1, 117.9, 117.0, 112.3, 68.0, 51.3, 50.2, 20.8; HRMS (ESI-TOF) m/z : $[\text{M}+\text{H}]^+$ calcd for $\text{C}_{23}\text{H}_{24}\text{N}_2\text{O}_3$, 376.1787; found, 376.1783.

Characterization of 2(6-methylpyridin-3-yl) (4(p-tolyl)piperazin-1-yl)methyl phenol (4q); Yellow solid; mp: 152–154 °C; 93% yield; ^1H NMR (CDCl_3 , 400MHz) δ : 11.61 (s, 1H), 8.51 (s, 1H), 7.75 (d, 1H, $J = 8\text{Hz}$), 7.17 (d, 1H, $J = 8\text{Hz}$), 7.12 (d, 1H, $J = \text{Hz}$), 7.07 (d, 2H, $J = 8\text{Hz}$), 6.94 (d, 1H, $J = 12\text{Hz}$), 6.89 (d, 1H, $J = 8\text{Hz}$), 6.81 (d, 2H, $J = 12\text{Hz}$), 6.76 (t, 1H, $J = 8\text{Hz}$), 4.51 (s, 1H), 3.21 (s, 4H), 2.62 (s, 4H), 2.53 (s, 3H), 2.27 (s, 3H); ^{13}C NMR (CDCl_3 , 100MHz) δ : 158.7, 156.4, 149.3, 148.7, 136.2, 132.2, 129.9, 129.8, 129.2, 129.1, 124.5, 123.9, 119.8, 117.3, 116.7, 73.3, 51.7, 49.9, 24.2, 20.5; HRMS (ESI-TOF) m/z : $[\text{M}+\text{H}]^+$ calcd for $\text{C}_{24}\text{H}_{27}\text{N}_3\text{O}$, 373.2154; found, 373.2151

Characterization of 1(5(4-chlorophenyl)piperazin-1-yl) (2-hydroxyphenyl)methyl thiophen-2-yl)ethanone (4r); Off-white solid; ^1H NMR (CDCl_3 , 400 MHz) δ : 10.98 (br-s, 1H) 7.60 (d, $J = 4\text{Hz}$, 1H) 7.27–7.20 (m, 4H) 7.04–7.02 (m, 1H) 6.94 (d, $J = 8\text{Hz}$, 1H) 6.87–6.81 (m, 3H) 4.83 (s, 1H) 3.22–3.33 (m, 4H) 2.83–2.55 (m, 4H) 2.55 (s, 3H); ^{13}C NMR (CDCl_3 , 100 MHz) δ : 190.4, 155.9, 150.5, 149.3, 144.3, 132.4, 129.6, 129.1, 128.9, 127.6, 125.3, 123.9, 119.9, 117.5, 117.4, 70.5, 51.1, 49.3, 26.7; LCMS m/z : $[\text{M}+\text{H}]^+$ calcd for $\text{C}_{23}\text{H}_{23}\text{ClN}_2\text{O}_2\text{S}$, 427.1247; found, 427.0009.

Alamar Blue assay: The potency of title compounds against MCF-7 cells was determined using the Alamar Blue assay, following the procedure described earlier [30–38]. Compounds were dissolved in DMSO at 10 mg/mL concentration and stored at -20°C . The dilutions were diluted in culture medium before treatment. A total of 10×10^3 cells/well were plated in 96-well plates. After 6 h of plating, the cells were treated with different concentrations of compound in triplicates. Reagent (20 μL of 5 mg/mL) was added to the cells during the last 4h of their time point for 48 h as per manufacturer's instructions. The medium was removed from the wells 4 h after the reagent addition, after which the absorbance was measured at 590 nm in an enzyme-linked immunosorbent assay reader.

In silico DFT calculations: The DFT calculations for the molecules (4a–4r) were carried out using B3LYP hybrid functional with 6-31 + g (d) all electron basis set utilizing the Gaussian 09 package [39]. All structures were optimized without any restraints. Partial Mulliken charges were calculated using the same level of theory to determine the charge distribution in the system. The electronic properties such as chemical hardness [$\eta = (\text{LUMO} - \text{HOMO})/2$], electronegativity [$\chi = -(\text{HOMO} + \text{LUMO})/2$], chemical potential [$\mu = (\text{H} + \text{L})/2$], and electrophilicity index ($\omega = \mu^2/2\eta$) were calculated using the energies of highest occupied molecular orbital (HOMO) and lowest unoccupied molecular orbital (LUMO). Chemical hardness (η) was used as a tool to understand the chemical reactivity of the molecular system. The concept of electronegativity (χ) is introduced as the power of an atom in a molecule to attract electrons onto itself. Electrophilicity (ω) is proposed as a measure of lowering of energy due to maximal electron flow between donor and acceptor.

Conclusively, the HOMO-LUMO (Δ) gap establishes the correlation between chemical structure and biological activity.

Western blot analysis: Western blot analysis was carried out by using the earlier reported protocol. pBad (Ser136: equivalent to human BADSer99) and hBAD antibodies were procured from Cell Signaling and similarly mouse anti- β -ACTIN from Santa Cruz Biotechnology [9].

4. Conclusions

In summary, from the synthesis of a series of novel NPB analogs using the Petasis reaction, based on their efficacy against mammary carcinoma cells, compounds such as 2(4(2,3-dichlorophenyl)piperazin-1-yl) (naphthalen-1-yl)methylphenol (**4e**), 5(4(2,3-dichlorophenyl)piperazin-1-yl) (2-hydroxyphenyl)methylfuran-2-carbaldehyde (**4f**), and 3(2-hydroxyphenyl) (4(p-tolyl)piperazin-1-yl)methylbenzaldehyde (**4i**) were found to inhibit the viability of mammary carcinoma cells. In addition, the crystal structure of the compound **4r**, which was grown via a slow-solvent evaporation technique, is reported. Furthermore, we identified that compounds **4f**, **4e** and **4i** decreased the phosphorylation of hBAD-Ser99. Such studies using NPB analogs will contribute to the lead optimization process of BAD phosphorylation inhibitors in oncology.

Supplementary Materials: The following are available online at <https://www.mdpi.com/article/10.3390/ijms222011002/s1>.

Author Contributions: S.S.G., D.D., A.S. and D.M.G., performed the work. M.M., G.P., K.S.R., V.P., B.B. and P.E.L. analyzed the data. B.B. and P.E.L. designed the work and wrote the manuscript. All authors have read and agreed to the published version of the manuscript.

Funding: This work was supported by the Council of Scientific and Industrial Research, DBT-NER, and Vision Group on Science and Technology (CESEM), Government of Karnataka. This work was also supported by the Shenzhen Key Laboratory of Innovative Oncotherapeutics (ZDSYS20200820165400003) (Shenzhen Science and Technology Innovation Commission), China; Shenzhen Development and Reform Commission Subject Construction Project ([2017]1434), China; Overseas Research Cooperation Project (HW2020008) (Tsinghua Shenzhen International Graduate School), China; Tsinghua University Stable Funding Key Project (WDZC20200821150704001); the Shenzhen Bay Laboratory (21310031), China and TBSI Faculty Start-up Funds, China. SGS thanks the University of Mysore for providing the SC/ST fellowship.

Acknowledgments: The authors thank Jerry Yang Jirui for technical assistance.

Conflicts of Interest: V.P., K.S.R., B.B. and P.E.L. are listed as inventors on a patent application for NPB (WO/2019/194520). P.E.L. is an equity holder in Sinotar Pharmaceuticals Ltd. which currently holds the license for this patent.

References

1. Fang, X.; Yu, S.; Eder, A.; Mao, M.; Bast, R.C., Jr.; Boyd, D.; Mills, G.B. Regulation of BAD phosphorylation at serine 112 by the Ras-mitogen-activated protein kinase pathway. *Oncogene* **1999**, *18*, 6635–6640. [[CrossRef](#)]
2. Zha, J.; Harada, H.; Osipov, K.; Jockel, J.; Waksman, G.; Korsmeyer, S.J. BH3 domain of BAD is required for heterodimerization with BCL-XL and pro-apoptotic activity. *J. Biol. Chem.* **1997**, *272*, 24101–24104. [[CrossRef](#)]
3. Wang, Y.; Chiou, Y.S.; Chong, Q.Y.; Zhang, M.; Rangappa, K.S.; Ma, L.; Zhu, T.; Kumar, A.P.; Huang, R.Y.; Pandey, V.; et al. Pharmacological Inhibition of BAD Ser99 Phosphorylation Enhances the Efficacy of Cisplatin in Ovarian Cancer by Inhibition of Cancer Stem Cell-like Behavior. *ACS Pharm. Transl. Sci.* **2020**, *3*, 1083–1099. [[CrossRef](#)] [[PubMed](#)]
4. Datta, S.R.; Brunet, A.; Greenberg, M.E. Cellular survival: A play in three Akts. *Genes Dev.* **1999**, *13*, 2905–2927. [[CrossRef](#)] [[PubMed](#)]
5. Bui, N.L.; Pandey, V.; Zhu, T.; Ma, L.; Basappa, B.; Lobie, P.E. Bad phosphorylation as a target of inhibition in oncology. *Cancer Lett.* **2018**, *415*, 177–186. [[CrossRef](#)]
6. Moody, S.E.; Schinzel, A.C.; Singh, S.; Izzo, F.; Strickland, M.R.; Luo, L.; Thomas, S.R.; Boehm, J.S.; Kim, S.Y.; Wang, Z.C.; et al. PRKACA mediates resistance to HER2-targeted therapy in breast cancer cells and restores anti-apoptotic signaling. *Oncogene* **2015**, *34*, 2061–2071. [[CrossRef](#)]
7. Tan, Y.; Demeter, M.R.; Ruan, H.; Comb, M.J. BAD Ser-155 phosphorylation regulates BAD/Bcl-XL interaction and cell survival. *J. Biol. Chem.* **2000**, *275*, 25865–25869. [[CrossRef](#)] [[PubMed](#)]

8. Zhou, X.M.; Liu, Y.; Payne, G.; Lutz, R.J.; Chittenden, T. Growth factors inactivate the cell death promoter BAD by phosphorylation of its BH3 domain on Ser155. *J. Biol. Chem.* **2000**, *275*, 25046–25051. [[CrossRef](#)]
9. Pandey, V.; Wang, B.; Mohan, C.D.; Raquib, A.R.; Rangappa, S.; Srinivasa, V.; Fuchs, J.E.; Girish, K.S.; Zhu, T.; Bender, A.; et al. Discovery of a small-molecule inhibitor of specific serine residue BAD phosphorylation. *Proc. Natl. Acad. Sci. USA* **2018**, *115*, E10505–E10514. [[CrossRef](#)]
10. Lobie, P.E.; Pandey, V.K.; Rangappa, K.S.; Basappa, M.; Chakrabhavi, D.; Rangappa, S.; Srinivasa, V. World Intellectual Property Organization. WO2018194520 A1, 25 October 2018.
11. Anusha, S.; Mohan, C.D.; Ananda, H.; Baburajeev, C.P.; Rangappa, S.; Mathai, J.; Fuchs, J.E.; Li, F.; Shanmugam, M.K.; Bender, A.; et al. Adamantyl-tethered-biphenylic compounds induce apoptosis in cancer cells by targeting Bcl homologs. *Bioorg. Med. Chem. Lett.* **2016**, *26*, 1056–1060. [[CrossRef](#)]
12. Priya, B.S.; Swamy, S.N.; Tejesvi, M.V.; Basappa, B.; Sarala, G.; Gaonkar, S.L.; Naveen, S.; Prasad, J.S.; Rangappa, K.S. Synthesis, characterization, antimicrobial and single crystal X-ray crystallographic studies of some new sulfonyl, 4-chloro phenoxy benzene and dibenzoazepine substituted benzamides. *Eur. J. Med. Chem.* **2006**, *41*, 1262–1270. [[CrossRef](#)]
13. Bharathkumar, H.; Mohan, C.D.; Ananda, H.; Fuchs, J.E.; Li, F.; Rangappa, S.; Surender, M.; Bulusu, K.C.; Girish, K.S.; Sethi, G.; et al. Microwave-assisted synthesis, characterization and cytotoxic studies of novel estrogen receptor α ligands towards human breast cancer cells. *Bioorg. Med. Chem. Lett.* **2015**, *25*, 1804–1807. [[CrossRef](#)] [[PubMed](#)]
14. Rangappa, K.; Basappa, B. New cholinesterase inhibitors: Synthesis and structure-activity relationship studies of 1,2-benzisoxazole series and novel imidazolyl-d 2-isoxazolines. *J. Phys. Org. Chem.* **2005**, *18*, 773–778. [[CrossRef](#)]
15. Basappa, B.; Kavitha, C.V.; Rangappa, K.S. Simple and an efficient method for the synthesis of 1-[2-dimethylamino-1-(4-methoxyphenyl)-ethyl]-cyclohexanol hydrochloride: (+/–) venlafaxine racemic mixtures. *Bioorg. Med. Chem. Lett.* **2004**, *14*, 3279–3281. [[CrossRef](#)]
16. Rakesh, K.S.; Jagadish, S.; Vinayaka, A.C.; Hemshekhar, M.; Paul, M.; Thushara, R.M.; Sundaram, M.S.; Swaroop, T.R.; Mohan, C.D.; Basappa, B.; et al. A new ibuprofen derivative inhibits platelet aggregation and ROS mediated platelet apoptosis. *PLoS ONE* **2014**, *9*, e107182. [[CrossRef](#)]
17. Naskar, D.; Roy, A.; Seibel, W.L.; Portlock, D.E. Novel Petasis boronic acid-Mannich reactions with tertiary aromatic amines. *Tetrahedron Lett.* **2003**, *44*, 5819–5821. [[CrossRef](#)]
18. Petasis, N.A.; Akritopoulou, I. The boronic acid mannich reaction: A new method for the synthesis of geometrically pure allylamines. *Tetrahedron Lett.* **1992**, *34*, 583–586. [[CrossRef](#)]
19. Rimpiläinen, T.; Nunes, A.; Calado, R.; Fernandes, A.S.; Andrade, J.; Ntungwe, E.; Spengler, G.; Szemerédi, N.; Rodrigues, J.; Gomes, J.P.; et al. Increased antibacterial properties of indoline-derived phenolic Mannich bases. *Eur. J. Med. Chem.* **2021**, *220*, 113459. [[CrossRef](#)] [[PubMed](#)]
20. Hommelsheim, R.; Núñez Ponce, H.M.; Truong, K.N.; Rissanen, K.; Bolm, C. 2-Sulfoximidoyl Acetic Acids from Multicomponent Petasis Reactions and Their Use as Building Blocks in Syntheses of Sulfoximine Benzodiazepine Analogues. *Org. Lett.* **2021**, *23*, 3415–3420. [[CrossRef](#)]
21. Potowski, M.; Esken, R.; Brunschweiler, A. Translation of the copper/bipyridine-promoted Petasis reaction to solid phase-coupled DNA for encoded library synthesis. *Bioorg. Med. Chem.* **2020**, *28*, 115441. [[CrossRef](#)]
22. Basappa, B.; Satish Kumar, M.; Nanjunda Swamy, S.; Mahendra, M.; Shashidhara Prasad, J.; Viswanath, B.S.; Rangappa, K.S. Novel delta2-isoxazolines as group II phospholipase A2 inhibitors. *Bioorg. Med. Chem. Lett.* **2004**, *14*, 3679–3681. [[CrossRef](#)] [[PubMed](#)]
23. *A.P.E.X. Bruker*; Bruker AXS Inc.: Madison, WI, USA, 2004.
24. Sheldrick, G.M. Crystal structure refinement with SHELXL. *Acta Crystallogr. C Struct. Chem.* **2015**, *71*, 3–8. [[CrossRef](#)] [[PubMed](#)]
25. Speak, A.L. Platon, An integrated tool for the analysis of the results of a single crystal structure determination. *Acta Crystallogr. Sect. A Found. Crystallogr.* **1990**, *46*, C34.
26. Gautam Desiraju, R.; Steiner, T. *The Weak Hydrogen Bond in Structural Chemistry and Biology*; Oxford University Press/International Union of Crystallography: Oxford, UK, 1999; Volume 9, pp. 1–507.
27. Basappa, B.; Pookunoth, B.C.; Kempasiddegowda, M.S.; Subbegowda, R.K.; Lobie, P.; Pandey, V. Novel Biphenyl Amines Inhibit Oestrogen Receptor (ER)- α in ER-Positive Mammary Carcinoma Cells. *Molecules* **2021**, *26*, 783. [[CrossRef](#)] [[PubMed](#)]
28. Zhang, M.; Wang, B.; Chong, Q.Y.; Pandey, V.; Guo, Z.; Chen, R.M.; Wang, L.; Wang, Y.; Ma, L.; Kumar, A.P.; et al. A novel small-molecule inhibitor of trefoil factor 3 (TFF3) potentiates MEK1/2 inhibition in lung adenocarcinoma. *Oncogenesis* **2019**, *8*, 65. [[CrossRef](#)] [[PubMed](#)]
29. Guéniche, N.; Hugué, A.; Bruyere, A.; Habauzit, D.; Le Hégarat, L.; Fardel, O. Comparative in silico prediction of P-glycoprotein-mediated transport for 2010–2020 US FDA-approved drugs using six Web-tools. *Biopharm. Drug Dispos.* **2021**, *42*, 393–398. [[CrossRef](#)]
30. Poh, H.M.; Chiou, Y.S.; Chong, Q.Y.; Chen, R.M.; Rangappa, K.S.; Ma, L.; Zhu, T.; Kumar, A.P.; Pandey, V.; Basappa, B.; et al. Inhibition of TFF3 Enhances Sensitivity-and Overcomes Acquired Resistance-to Doxorubicin in Estrogen Receptor-Positive Mammary Carcinoma. *Cancers* **2019**, *11*, 1528. [[CrossRef](#)]
31. Gilandoust, M.; Harsha, K.B.; Mohan, C.D.; Raquib, A.R.; Rangappa, S.; Pandey, V.; Lobie, P.E.; Basappa, B.; Rangappa, K.S. Synthesis, characterization and cytotoxicity studies of 1,2,3-triazoles and 1,2,4-triazolo [1,5-a] pyrimidines in human breast cancer cells. *Bioorg. Med. Chem. Lett.* **2018**, *28*, 2314–2319. [[CrossRef](#)]

32. Chong, Q.Y.; You, M.L.; Pandey, V.; Banerjee, A.; Chen, Y.J.; Poh, H.M.; Zhang, M.; Ma, L.; Zhu, T.; Basappa, S.; et al. Release of HER2 repression of trefoil factor 3 (TFF3) expression mediates trastuzumab resistance in HER2+/ER+ mammary carcinoma. *Oncotarget* **2017**, *8*, 74188–74208. [[CrossRef](#)]
33. Kumar, C.A.; Jayarama, S.; Basappa, B.; Salimath, B.P.; Rangappa, K.S. Pro-apoptotic activity of imidazole derivatives mediated by up-regulation of Bax and activation of CAD in Ehrlich Ascites Tumor cells. *Invest. New Drugs* **2007**, *25*, 343–350. [[CrossRef](#)]
34. Anusha, S.; Anandakumar, B.S.; Mohan, C.D.; Nagabhushana, G.P.; Priya, B.S.; Rangappa, K.S.; Basappa, B.; Chandrappa, G.T. Preparation and use of combustion-derived Bi₂O₃ for the synthesis of heterocycles with anti-cancer properties by Suzuki-coupling reactions. *RSC Adv.* **2014**, *4*, 52181–52188.
35. Ravi Kumar, K.R.; Mallesha, H.; Basappa, R.K.S. Synthesis of novel isoxazolidine derivatives and studies for their antifungal properties. *Eur. J. Med. Chem.* **2003**, *38*, 613–619. [[CrossRef](#)]
36. Bharathkumar, H.; Paricharak, S.; Dinesh, K.R.; Siveen, K.S.; Fuchs, J.E.; Rangappa, S.; Mohan, C.D.; Mohandas, N.; Kumar, A.P.; Sethi, G.; et al. Synthesis, biological evaluation and in silico and in vitro mode-of-action analysis of novel dihydropyrimidones targeting PPAR- γ . *RSC Adv.* **2014**, *4*, 45143–45146. [[CrossRef](#)]
37. Basappa, B.; Rangappa, K.S.; Sugahara, K. Roles of glycosaminoglycans and glycanmimetics in tumor progression and metastasis. *Glycoconj. J.* **2014**, *31*, 461–467. [[CrossRef](#)] [[PubMed](#)]
38. Blanchard, V.; Chevalier, F.; Imberty, A.; Leeftang, B.R.; Basappa, B.; Sugahara, K.; Kamerling, J.P. Conformational studies on five octasaccharides isolated from chondroitin sulfate using NMR spectroscopy and molecular modeling. *Biochemistry* **2007**, *46*, 1167–1175. [[CrossRef](#)] [[PubMed](#)]
39. Frisch, M.J.; Trucks, G.W.; Schlegel, H.B.; Scuseria, G.E.; Robb, M.A.; Cheeseman, J.R.; Scalmani, G.; Barone, V.; Petersson, G.A.; Nakatsuji, H.; et al. *Gaussian 16, Revision, C.01*; Gaussian, Inc.: Wallingford, CT, USA, 2016.